

FINITE VOLUME SOLUTION OF BOUSSINESQ-TYPE EQUATIONS ON AN UNSTRUCTURED GRID

Walid El Asmar¹ and Okey Nwogu¹

A new numerical method is developed to solve a set of two-dimensional Boussinesq water wave evolution equations over an unstructured grid. The governing mass and momentum conservation equations are discretized over an irregular triangular grid, with a staggered placement of the variables. The free surface elevation is defined at the centroid of the triangles, while the normal component of the velocity is defined at the mid-point of the triangle edges. The mass conservation equation is then integrated over a control volume defined over each triangle while the momentum equations are integrated over a control volume formed from two adjacent triangles. A modified Crank-Nicolson scheme is used to integrate the equations in time. Two numerical experiments are used to evaluate the conservation properties and accuracy of the numerical method: solitary wave propagation in a curved channel, and interaction of solitary waves with a vertical circular cylinder.

1. INTRODUCTION

Numerical models that solve Boussinesq-type water wave evolution equations are commonly used to investigate surface wave propagation and transformation in coastal regions. Most of the models use finite difference schemes to discretize the equations over uniformly-spaced rectangular grids (e.g. Abbott *et al.*, 1978; Wei and Kirby, 1995; Nwogu and Demirbilek, 2001). The popularity of finite difference schemes is largely based on their simplicity and ease of implementation. However, the use of structured grids can severely restrict the potential application of such models to complex boundary problems such as coastal flooding over complex topography, wave propagation in curved channels, wave interaction with coastal structures of arbitrary shape, and wave agitation in harbors of arbitrary shape. Unstructured grids provide users the flexibility of modeling complex geometries. In addition, the grid resolution can be refined where needed such as near structures or in shallow regions.

Several techniques have been developed to solve Boussinesq-type equations over irregular shaped domains. Wang *et al.* (1992) and Shi *et al.* (2001) developed curvilinear-grid based finite difference schemes. The curvilinear grid approach offers the simplicity of structured grid schemes while improving their flexibility. However, curvilinear methods might have mapping problems for complex grid geometries. Hence, their application remains limited to computational domains with relatively simple boundaries.

¹ Dept. of Naval Arch. and Marine Eng., University of Michigan, Ann Arbor, MI, 48109-2145, USA

Finite element solution schemes for Boussinesq equations have been developed by Antunes do Carmo *et al.* (1993), Ambrosi and Quartapelle (1998), Walkley and Berzins (2002), Woo and Liu (2004) and others. Compared to structured finite difference schemes, the adoption of an unstructured grid can add considerable difficulty to the discretization of the equations, treatment of the third-order spatial derivative terms that govern the dispersive properties of the equations, and change the conservation properties of the discretized equations. Walkley and Berzins (2002), for example, showed that large local variations in mesh size, or the existence of dominant orientations of the cell faces could have a noticeable impact on the numerical solution.

Classical finite volume schemes that are commonly used to solve the shallow water equations have also been modified to solve Boussinesq-type equations. Soares-Frazão and Zech (2002) proposed a “hybrid finite-volume scheme”, where the dispersive terms are considered to be forcing terms and placed on the right-hand of the equations. The finite volume method is used to solve the shallow water part of the equations with the dispersive forcing terms evaluated using a finite difference scheme. Bradford and Sanders (2002) proposed a two-step approach. They initially neglect the dispersive terms, thus solving the shallow water equations. The temporary solutions are then used to estimate the dispersive effects and obtain new values for the main variables. Hybrid finite volume schemes that do not include the dispersive terms as an integral part of the solution are bound to have convergence problems in deeper water as the effects of frequency dispersion become relatively more important.

An important consideration in the development of unstructured grid schemes for Boussinesq-type equations with either finite element or finite volume methods is the stability of the numerical scheme. Placement of the water surface elevation and velocity variables at the element nodes can lead to spurious numerical oscillations that would require filtering and/or other stabilization measures. Spurious numerical oscillations can be avoided by using the staggered mesh concept of Harlow and Welch (1965). Although staggered meshes locally conserve mass, momentum and energy on structured Cartesian grids, local conservation is not necessarily guaranteed for unstructured grids. Perot (2000), however, demonstrated that it is feasible to achieve local conservation of mass, momentum, kinetic energy and circulation with certain staggered-mesh unstructured grids. His approach relies on the concept of the dual orthogonal mesh (Delaunay/Voronoi tessellation). A staggered-grid finite volume method for solving the Euler equations that does not rely on creating a dual Delaunay-Voronoi mesh was proposed by Wenneker *et al.* (2002). Wenneker *et al.* (2003) later demonstrated that the scheme also conserves mass, momentum and energy.

In this paper, a consistent finite volume method is developed to solve a set of two-dimensional Boussinesq-type water wave evolution equations on an irregular triangular grid using an approach similar to that of Wenneker *et al.* (2002). In contrast to previous finite element and finite volume Boussinesq

solvers where both the free surface elevation and two components of the horizontal velocities are co-located at the nodes of the elements, we adopt a staggered placement of the variables. The mass conservation equation is integrated over a control volume defined over each triangle while the momentum equations are integrated over a control volume formed from two adjacent triangles. A reconstruction scheme is used to retrieve the full velocity vector at the vertices of the triangles. The numerical model is used to investigate the propagation of solitary waves in a curved channel, and interaction of solitary waves with a vertical circular cylinder.

2. NUMERICAL METHOD

Governing Equations

The governing equations are the weakly-nonlinear set of Boussinesq-type mass and momentum conservation equations derived by Nwogu (1993). The depth-integrated mass conservation equation can be written as:

$$\eta_t + \nabla \cdot \mathbf{Q} = 0 \quad (1)$$

where $\nabla = (\partial/\partial x, \partial/\partial y)$, $\eta(\mathbf{x}, t)$ is the water surface elevation and $\mathbf{Q}(\mathbf{x}, t)$ is the volume flux density given by:

$$\mathbf{Q} = \int_{-h}^{\eta} \mathbf{u} dz = (h + \eta) \mathbf{u}_\alpha + h \left\{ \left[\frac{(z_\alpha + h)^2}{2} - \frac{h^2}{6} \right] \nabla (\nabla \cdot \mathbf{u}_\alpha) + \left[(z_\alpha + h) - \frac{h}{2} \right] \left[\nabla (\mathbf{u}_\alpha \cdot \nabla h) + (\nabla \cdot \mathbf{u}_\alpha) \nabla h \right] \right\} \quad (2)$$

where h is the water depth, \mathbf{u}_α is the horizontal velocity at a reference elevation $z = z_\alpha$ in the water column. The momentum equation is given by:

$$\mathbf{u}_{\alpha,t} + g \nabla \eta + (\mathbf{u}_\alpha \cdot \nabla) \mathbf{u}_\alpha + z_\alpha \left[\nabla (\mathbf{u}_{\alpha,t} \cdot \nabla h) + (\nabla \cdot \mathbf{u}_{\alpha,t}) \nabla h \right] + \frac{1}{2} \left[(z_\alpha + h)^2 - h^2 \right] \nabla (\nabla \cdot \mathbf{u}_{\alpha,t}) = 0 \quad (3)$$

where g is the gravitational acceleration. The elevation of the velocity variable z_α is chosen to minimize differences between the linear dispersion characteristics of the model and the exact dispersion relation for small amplitude waves and is given by $z_\alpha = -0.535h$ (Nwogu, 1993).

Grid Topology and Placement of Variables

A staggered placement of the variables is adopted as shown in Fig. 1. The water surface elevation is defined at the centroids of the triangles, while the normal component of the velocity is defined at the midpoints of the triangle edges. The velocities at the cell faces are assumed to be continuous in contrast to standard shallow water finite volume schemes that allow for discontinuous

velocities at cell faces.

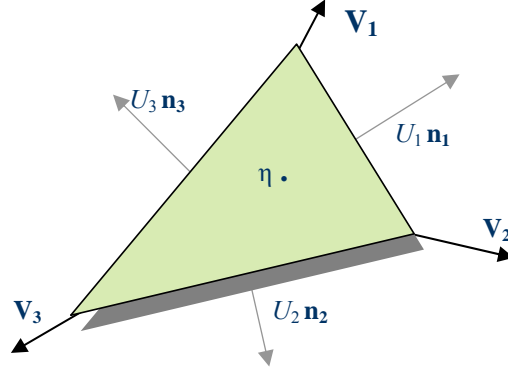


Figure 1. Staggered placement of variables on a triangular grid.

Control Volume Integrated Equations

The control volume used for the mass conservation equation consists of a single triangular cell. The mass equation (Eq. 1) is integrated over the control volume to yield:

$$\frac{\partial}{\partial t} \int_{\Omega_\beta} \eta \, d\Omega = - \int_{\Omega_\beta} \nabla \cdot \mathbf{Q} \, d\Omega \quad (4)$$

where Ω_β is the surface area of cell β . The control volume for the momentum equation is composed of two adjacent grid cells (see Fig. 2). The momentum equation is initially projected in the direction normal to the common edge, and then integrated over the combined control volume area. The control volume-integrated momentum equation for water of constant depth is given by:

$$\begin{aligned} & \frac{\partial}{\partial t} \left(\int_{\Omega_E} \mathbf{u}_\alpha \cdot \mathbf{N}_E \, d\Omega + \alpha h^2 \int_{\Omega_E} \nabla (\nabla \cdot \mathbf{u}_\alpha) \cdot \mathbf{N}_E \, d\Omega \right) \\ & - g \int_{\Omega_E} \nabla \eta \cdot \mathbf{N}_E \, d\Omega - \int_{\Omega_E} \nabla (\mathbf{u}_\alpha \cdot \mathbf{u}_\alpha) \cdot \mathbf{N}_E \, d\Omega = 0 \end{aligned} \quad (5)$$

where β and γ denote adjacent cells, $\alpha = -0.392$, \mathbf{N}_E is the unit normal vector to common edge, and $\Omega_E = \Omega_\beta + \Omega_\gamma$ is the surface area of the control volume. The advection term in Eq. (5) has been modified by assuming the flow to be irrotational in the horizontal plane, i.e. $(\mathbf{u}_\alpha \cdot \nabla) \mathbf{u}_\alpha = \nabla (\mathbf{u}_\alpha \cdot \mathbf{u}_\alpha)$. The projected momentum equation is independent of the choice of direction for \mathbf{N}_E . A simple convention used in this paper is to define a unique direction for \mathbf{N}_E by orienting all unit normal vectors away from the origin of the coordinate system.

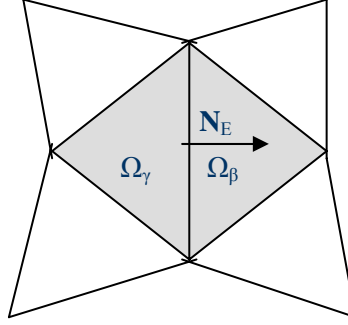


Figure 2. Control volume of integrated momentum equation.

Evaluation of Area Integrals

In order to numerically evaluate the mass conservation equation (Eq. 4), the divergence theorem is used to convert the area integral of the volume flux term into a line integral along the triangle edges. The water surface elevation is assumed to be constant over the area of the cell and defined at the centroid of the cell, while the flux terms are assumed to be constant along the cell edges and defined at the mid-point of the cell edges. The mass conservation equation then becomes:

$$\Omega_\beta \frac{\partial \eta_\beta}{\partial t} = - \sum_{i=1}^3 l_i \left((h + \eta)_i U_i - \left(\alpha + \frac{1}{3} \right) h_i^3 [\nabla(\nabla \cdot \mathbf{u}_\alpha) \cdot \mathbf{n}_i] \right) \quad (6)$$

where η_β is the water surface elevation at the centroid of cell β , l_i are the lengths of the sides of cell i , \mathbf{n}_i are their respective outward unit normal vectors, and $U_i = \mathbf{u}_\alpha \cdot \mathbf{n}_i$ is the outward normal component of the velocity \mathbf{u}_α at the midpoint of cell edge i .

The values of η at the cell edges are estimated using a weighted average of the values of η at the centroids of neighboring cells:

$$\eta_i = \psi_\beta \eta_\beta + \psi_\gamma \eta_\gamma \quad (7)$$

The weighting coefficients ψ_β, ψ_γ are calculated based on the relative distance of the centroids $[(x_\beta, y_\beta), (x_\gamma, y_\gamma)]$ from the midpoint of the cell edge:

$$\psi_\beta = \frac{x_\gamma(x_\gamma - x_\beta) + y_\gamma(y_\gamma - y_\beta)}{(x_\gamma - x_\beta)^2 + (y_\gamma - y_\beta)^2 + (x_\beta y_\gamma - x_\gamma y_\beta)^2} \quad (8)$$

$$\psi_\gamma = \frac{x_\beta(x_\beta - x_\gamma) + y_\beta(y_\beta - y_\gamma)}{(x_\beta - x_\gamma)^2 + (y_\beta - y_\gamma)^2 + (x_\gamma y_\beta - x_\beta y_\gamma)^2}$$

The second term on the right hand side of Eq. (6) represents the dispersive term in the mass conservation equation. It requires the evaluation of the projected

value of the gradient of the divergence of the velocity vector ($\nabla(\nabla \cdot \mathbf{u}_\alpha)$) along the cell edges. The divergence theorem is initially used to approximate $\nabla \cdot \mathbf{u}_\alpha$ as a scalar quantity defined at the centroid of the cells:

$$\nabla \cdot \mathbf{u}_\alpha = \frac{1}{\Omega} \sum_{i=1}^3 l_i U_i \quad (9)$$

By making use of the vector identity $\nabla f \cdot \mathbf{A} = \nabla \cdot (f\mathbf{A}) - f \nabla \cdot \mathbf{A}$ and the divergence theorem, the dispersive term is then evaluated as:

$$\nabla(\nabla \cdot \mathbf{u}_\alpha) \cdot \mathbf{n}_i = \frac{1}{\Omega} \sum_{j=1}^4 l_j (\nabla \cdot \mathbf{u}_\alpha)_j (\mathbf{n}_j \cdot \mathbf{n}_i) \quad (10)$$

The values of $\nabla \cdot \mathbf{u}_\alpha$ along the cell edges are obtained from the centroidal values using the scalar reconstruction scheme given in Eq. (7).

The divergence theorem is also used to transform the momentum equation:

$$\Omega_E \frac{\partial}{\partial t} U_E + \alpha h^2 \sum_{i=1}^4 l_i \frac{\partial}{\partial t} (\nabla \cdot \mathbf{u}_\alpha)_i (N_E \cdot \mathbf{n}_i) = - \sum_{i=1}^4 l_i [g \eta_i + (\mathbf{u}_\alpha \cdot \mathbf{u}_\alpha)_i] (N_E \cdot \mathbf{n}_i) \quad (11)$$

It should be noted that the dispersive term in the momentum equation (second term on the left hand side of Eq. 11) can yield up to thirteen normal velocity components corresponding to five edges of the two adjacent cells of the surface of integration, and eight additional edges from cells adjoining the surface of integration.

The velocity-squared term at the mid-point of the cell edges ($\mathbf{u}_\alpha \cdot \mathbf{u}_\alpha$) is approximated as the average of the values at the neighboring nodes. The full velocity vectors at the nodes are reconstructed from the normal components of the velocity at the midpoints of all the edges that connect to the node using the least-squares minimization scheme of Dukowicz and Meltz (1992). The scheme minimizes the difference, f , between the projected nodal velocity \mathbf{u} in the normal direction to the face and the actual normal velocity at the face:

$$f = \sum_{i=1}^k \psi_i [\mathbf{u} \cdot \mathbf{n}_i - U_i]^2 \quad (12)$$

where ψ_i are empirically assigned weighting coefficients and k is the number of edges that connect to the node. If all weighting coefficients are assigned a value of one, the least-squares solution is given by:

$$\mathbf{u} = \frac{1}{4ab - c^2} \begin{bmatrix} ce - 2bd \\ cd - 2ae \end{bmatrix} \quad (13)$$

$$\text{where } a = \sum_{i=1}^k \psi_i (n_i^x)^2 \quad b = \sum_{i=1}^k \psi_i (n_i^y)^2 \quad c = \sum_{i=1}^k 2\psi_i n_i^x n_i^y \\ d = - \sum_{i=1}^k 2\psi_i n_i^x U_i \quad e = - \sum_{i=1}^k 2\psi_i n_i^y U_i$$

The ψ coefficients can also be used to enforce Dirichlet boundary conditions at boundary nodes. This is done, for example, by assigning the coefficients of the inner faces a value of one, and the coefficients of the boundary faces a value much greater than one.

Time Integration

The mass and momentum equations are integrated in time using an iterative Crank-Nicolson scheme with a predictor-corrector scheme used to provide an initial guess. The scheme consists of three stages. At every time step $t = n\Delta t$, a predictor scheme is used to calculate the values of the variables at $t = (n+1/2)\Delta t$. These values are used in the following corrector stage to calculate the values of the variables at $t = (n+1)\Delta t$; which are then used as an initial guess in an iterative Crank-Nicolson scheme. A summary of the approach is provided in Table 1 below.

Table 1. Summary of Crank-Nicolson scheme.

	Water Surface Elevation	Normal Component of Velocity
Predictor	$\underline{\eta}^{n+\frac{1}{2}} = \underline{\eta}^n + \frac{\Delta t}{2} f_c(\underline{\eta}^n, \underline{U}^n)$	$\underline{U}^{n+\frac{1}{2}} = \underline{U}^n + \frac{\Delta t}{2} \mathbf{A}^{-1} f_m(\underline{\eta}^n, \underline{U}^n)$
Corrector	$\underline{\eta}^{n+1} = \underline{\eta}^n + \Delta t f_c(\underline{\eta}^{n+\frac{1}{2}}, \underline{U}^{n+\frac{1}{2}})$	$\underline{U}^{n+1} = \underline{U}^n + \Delta t \mathbf{A}^{-1} f_m(\underline{\eta}^{n+\frac{1}{2}}, \underline{U}^{n+\frac{1}{2}})$
Iterative	$\underline{\eta}^{n+1} = \underline{\eta}^n + \Delta t f_c(\underline{\eta}^{n+\frac{1}{2}}, \underline{U}^{n+\frac{1}{2}})$	$\underline{U}^{n+1} = \underline{U}^n + \Delta t \mathbf{A}^{-1} f_m(\underline{\eta}^{n+\frac{1}{2}}, \underline{U}^{n+\frac{1}{2}})$
	where $\underline{\eta}^{n+\frac{1}{2}} = \frac{1}{2}(\underline{\eta}^n + \underline{\eta}^{n+1})$, $\underline{U}^{n+\frac{1}{2}} = \frac{1}{2}(\underline{U}^n + \underline{U}^{n+1})$	

The matrix \mathbf{A} is constructed from the left hand side of the discretized momentum equation. The matrix is relatively sparse with each row containing a maximum of 13 non-zero entries. Two sparse matrix solvers were implemented, the Generalized Minimum Residual (GMRES) method and the Successive Overrelaxation (SOR) scheme.

3. NUMERICAL RESULTS

Propagation of Solitary Waves in Curved Channels

Shi *et al.* (1998) investigated the propagation of solitary waves through curved channels using a curvilinear finite difference method. Their work focused on the effect of channel width and bending sharpness on the reflected and transmitted waves. We consider one of Shi *et al.*'s numerical experiments involving a curved channel with a smooth 90° bend. The channel is $5h$ wide and

has an inner radius of $10h$ at the bend. The channel's upstream and downstream legs are both $100h$ long.

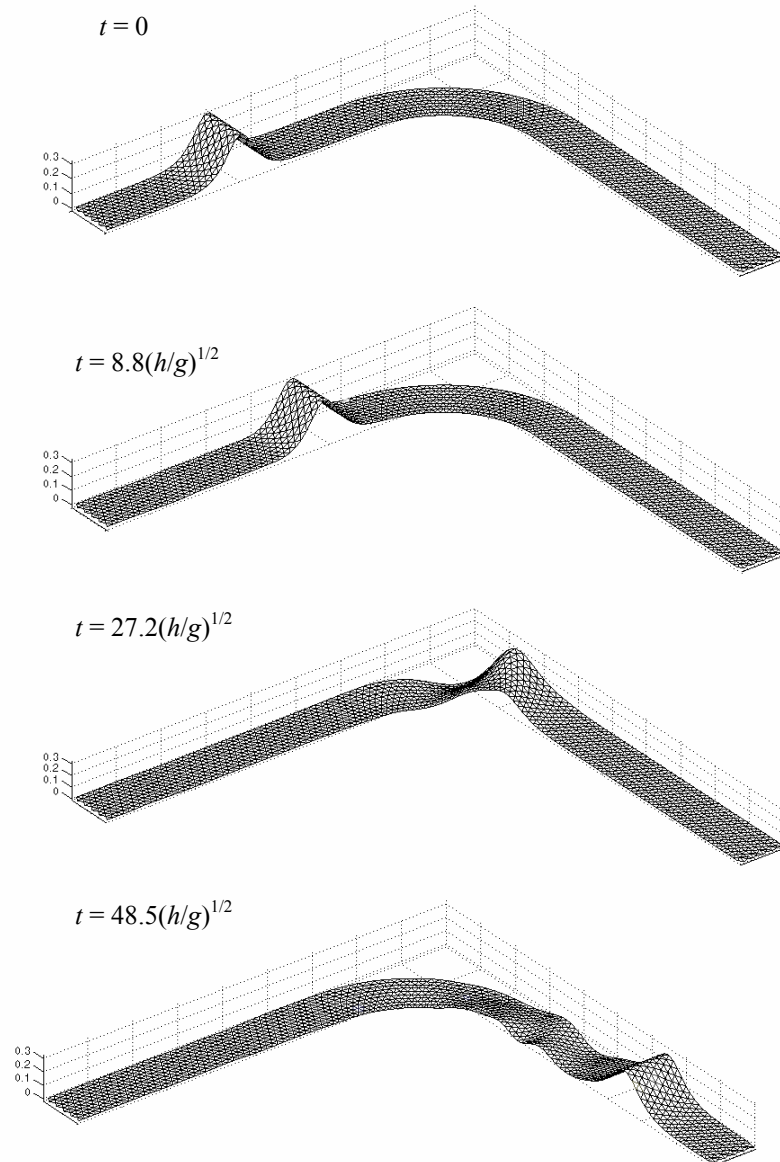


Figure 3. Snapshots of the predicted wave patterns for solitary wave propagation in a curved channel ($w = 5h$).

The computational domain was discretized into irregular triangular cells with side lengths $\Delta l \approx h$. A solitary wave of height $H=0.3h$ was initially placed at a distance $x = 85h$ from the upstream edge of the channel. The solitary wave profile was obtained from a Fourier series solution of the Boussinesq equations. Numerical simulations were performed with time step size $\Delta t = 0.05(h/g)^{1/2}$ for a duration of $48.5(h/g)^{1/2}$. The predicted wave patterns are shown in Figure 3. Wave reflection from the outer wall of the bend leads to a larger wave elevation in that corner as the waves propagate around the bend. The wave front in the outer corner also accelerates, eventually catching up with the slower waves in the inner corner to form a uniform crest in the downstream section. The predicted wave patterns are similar to those presented in Shi *et al.* (1998).

The transmitted wave profile at $t = 48.5(h/g)^{1/2}$ is shown in Figure 4. The transmitted wave had an amplitude of $0.259h$ with its crest is located at $x = 133h$. Shi *et al.* predicted an amplitude of $0.276h$ with the crest located at $x = 136h$. Both results are comparable, given the different form of Boussinesq equations employed by Shi *et al.* (1998), as well as differences in the numerical scheme.

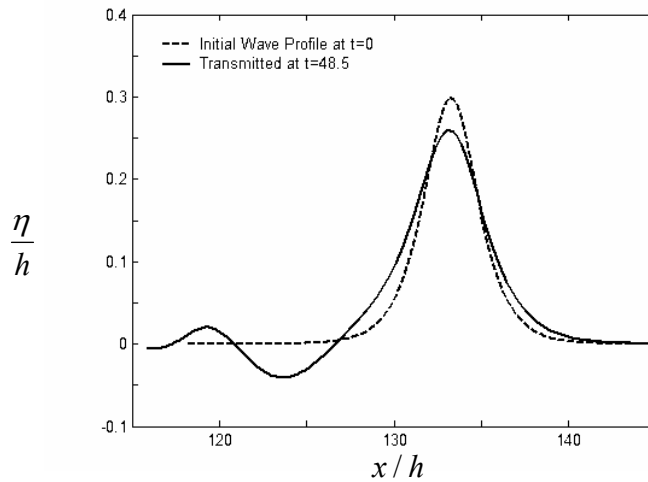


Figure 4. Initial and transmitted wave profile at $t = 48.5(h/g)^{1/2}$.

The simulations were repeated for a wider channel with a width of $10h$. The channel width is now comparable to the solitary wavelength ($\lambda = 2\pi/(3H/4h^3)^{1/2} \approx 13h$). The predicted wave patterns are shown in Fig. 5. For the wider channel, the phasing between the incident and reflected waves at the bend leads to a much larger crest elevation ($\sim 1.5H$) at the outer corner. The transmitted wave height ($0.18h$) is smaller compared to the narrower channel results. The transmitted wave profile is also no longer uniform across the crest and has larger trailing waves.

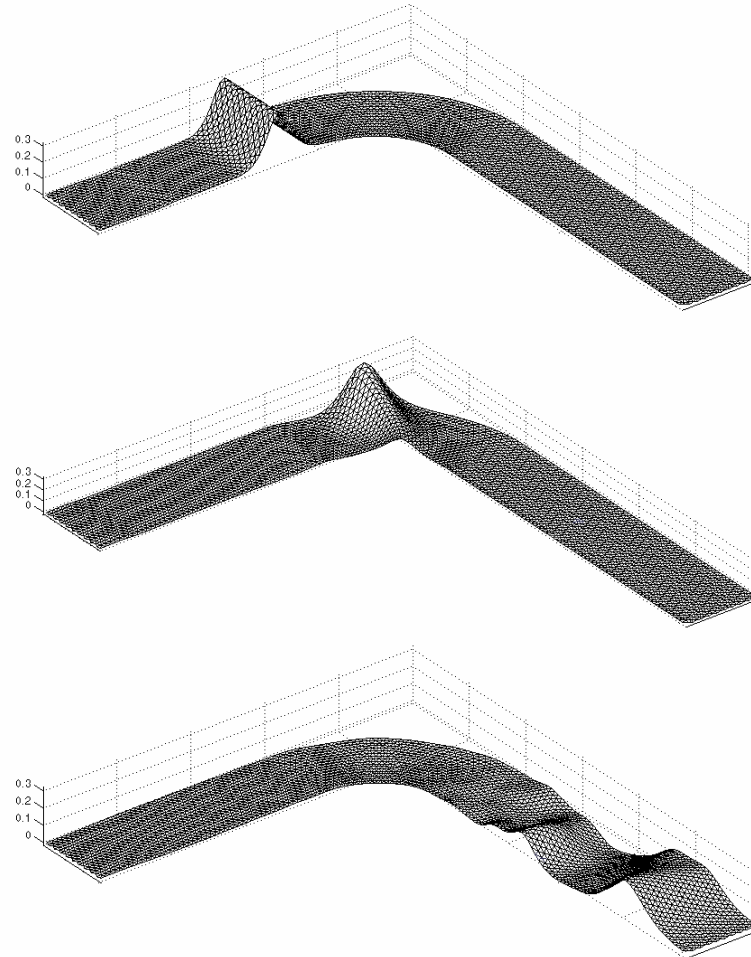


Figure 5. Snapshots of the predicted wave patterns for solitary wave propagation in a curved channel ($w = 10h$).

Solitary Wave Interaction with a Vertical Circular Cylinder

Antunes do Carmo *et al.* (1993) conducted laboratory experiments to investigate the interaction of a solitary wave with a vertical cylinder. The wave flume was 9 m long, 0.55 m wide and had a water depth of 0.15m. A 0.16m-diameter circular cylinder was installed in the middle of the flume. The center of the cylinder was located at $x = 4.5\text{m}$, $y = 0.275\text{m}$ relative to an origin defined at the lower corner of the upstream end of the flume. Six wave probes were used to measure the water surface elevation at the following locations: Gauge 1 = (4.400, 0.275), Gauge 2 = (4.500, 0.170), Gauge 3 = (4.500, 0.045), Gauge 4 = (4.600, 0.275), Gauge 5 = (4.975, 0.275), and Gauge 6 = (5.375, 0.275).

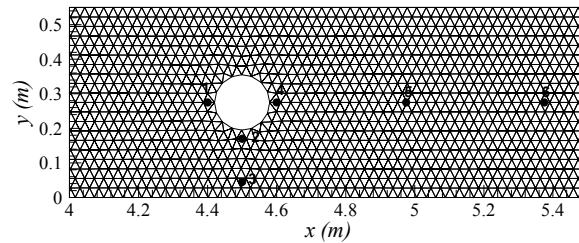


Figure 6. Triangular mesh used for solitary wave-cylinder interaction test.

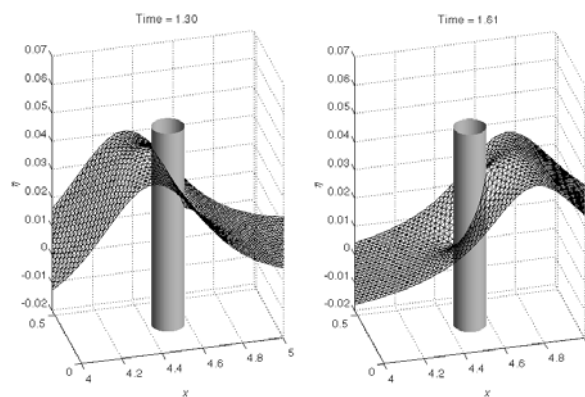


Figure 7. 3-D view of solitary wave interaction with cylinder.

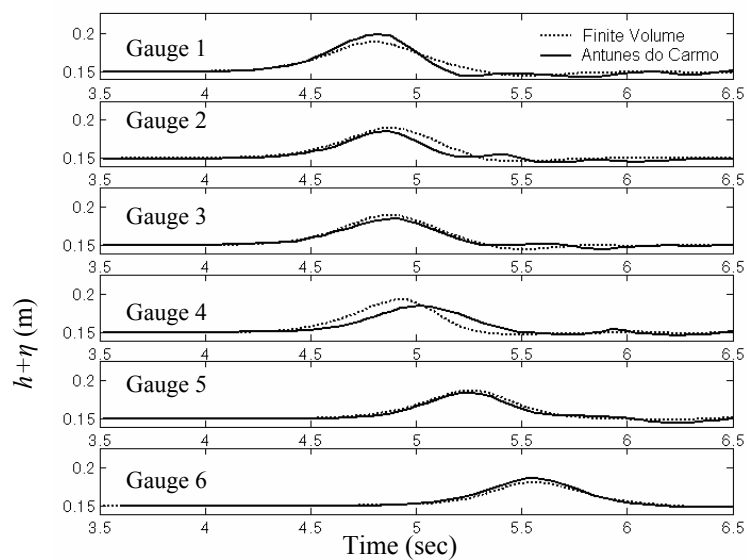


Figure 8. Measured and predicted time histories for solitary wave-cylinder interaction test.

A numerical flume was set up to reproduce the laboratory experiments. The 9m by 0.55m tank was discretized into triangles with side lengths of the order of 0.03m as shown in Fig. 6. A solitary wave with height $H = 0.0375\text{m}$ was generated inside a tank. Numerical simulations were performed for duration of 6.5s at a time step of 0.008s.

Snapshots of the wave-cylinder interaction are shown in Fig. 7 while the predicted and measured surface water elevation time histories are compared in Fig. 8. Reasonable agreement is observed between the numerical and experimental results at Gauges 3, 5 and 6, which are located farthest from the cylinder. Greater discrepancies are seen at Gauges 1, 2 and 4, which are in the immediate vicinity of the cylinder. Antunes do Carmo *et al.* (1993) obtained similar amplitude and phase shifts with their finite element Boussinesq model. Wu (2004) obtained better model-data comparisons with a Navier-Stokes solver. We suspect that the phase differences are related to numerical and analytical errors in the weakly nonlinear model phase speeds and plan to repeat the tests on a finer mesh grid with a fully nonlinear Boussinesq solver.

4. CONCLUSIONS

A new numerical method has been developed to solve Boussinesq-type water wave evolution equations over an unstructured grid. The scheme is based on the finite volume concept where the governing mass and momentum equations are integrated over local control volumes in order to locally satisfy the conservation laws. A staggered placement of the surface elevation and velocity variables is adopted to avoid spurious numerical oscillations and ensure stability. The scheme solves for the normal velocities along cell edges, as opposed to the two velocity components, making it relatively more computationally efficient. Preliminary numerical experiments have been conducted for solitary wave propagation in a curved channel and solitary wave interaction with a circular cylinder. The tests have demonstrated the viability of the staggered unstructured grid approach. Additional work is currently being performed to extend the model to the fully nonlinear Boussinesq equations.

ACKNOWLEDGMENTS

This work was supported in part by Michigan Sea Grant College Program under Grant No. NA16RG1145 from the National Sea Grant College program, and the Coastal Inlets Research Program of the U.S. Army Engineer Research and Development Center. The authors would like to thank Tso-Ren Wu for providing data from the wave-cylinder interaction experiment.

REFERENCES

- Abbott, M. B., Petersen, H. M., and O. Skovgaard. 1978. On the numerical modelling of short waves in shallow water, *J. Hyd. Res.*, **16**, 173-203.
- Ambrosi D., and L. Quartapelle. 1998. A Taylor-Galerkin method for simulating nonlinear dispersive water waves, *J. Comp. Phys.*, **146**, 546-569.

- Antunes do Carmo, J. S., Seabra-Santos, F. J. and E. Barthélemy. 1993. Surface waves propagation in shallow-water: A finite element model, *Int. J. Num. Methods Fluids*, **16**, 447 – 459.
- Bradford, S. F., and B. F. Sanders. 2002. Finite-volume models for unidirectional nonlinear dispersive waves, *ASCE Journal of Waterway, Port, Coastal and Ocean Engineering*, **128**, 173-182.
- Dukowicz, J. K., and B. J. A. Meltz. 1992, Vorticity errors in multidimensional Lagrangian codes, *J. Comp. Phys.*, **99**, 115-134.
- Harlow, F. H., and J. E. Welch. 1965. Numerical calculations of time dependent viscous incompressible flow of fluid with a free surface, *Physics of Fluids*, **8**, 2182-2189.
- Nwogu, O. 1993. Alternative form of Boussinesq equations for nearshore wave propagation, *ASCE Journal of Waterway, Port, Coastal and Ocean Engineering*, **119**, 618-638.
- Nwogu, O.G., and Demirbilek, Z. 2001. BOUSS-2D: A Boussinesq Wave Model for Coastal Regions and Harbors. ERDC/CHL Technical Report TR-01-25, U.S. Army Engineer Res. and Dev. Center, Vicksburg, MS.
- Perot, B. 2000. Conservation properties of unstructured staggered mesh schemes, *J. Comp. Phys*, **159**, 58–89.
- Shi, A., Teng, M.H. and T.Y. Wu. 1998. Propagation of solitary waves through significantly curved shallow water channels, *J. Fluid Mech.*, **362**, 157-176.
- Shi, F., Dalrymple, R.A., Kirby, J.T., Chen, Q., and A. Kennedy. 2001. A fully nonlinear Boussinesq model in generalized curvilinear coordinates, *Coastal Engineering*, **42**, 337-358.
- Soares-Frazão, S., and Y. Zech. 2002. Undular bores and secondary waves, experiments and hybrid finite-volume modeling, *J. Hyd. Res.*, **40**, 33-43.
- Walkley, M., and M. Berzins. 2002. A finite element model for the two-dimensional extended Boussinesq equations, *Int. J. Num. Methods Fluids*, **39**, 865-885.
- Wang, K. H., Wu, T. Y., and G. T. Yates. 1992. Three-dimensional scattering of solitary waves by vertical cylinder, *J. Waterway, Port, Coastal and Ocean Eng.*, **118**, 551-566.
- Wei, G., and J.T. Kirby. 1995. Time-dependent numerical code for extended Boussinesq equations, *J. Waterway, Port, Coastal and Ocean Eng.*, **121**, 251-261.
- Wenneker, I., Segal, A., and P. Wesseling. 2002. A Mach-uniform unstructured staggered grid method, *Int. J. Num. Methods Fluids*, **39**, 1209-1235.
- Wenneker, I., Segal, A., and P. Wesseling. 2003. Conservation properties of a new unstructured staggered scheme, *Computers and Fluids*, **32**, 139-147.
- Woo, S.-B., and P.L.-F. Liu. 2001. A Petrov-Galerkin finite element model for one-dimensional fully nonlinear and weakly dispersive wave propagation, *Int. J. Num. Methods Fluid*, **37**, 541-575.
- Wu, T.-S. 2004. A numerical study of three-dimensional breaking waves and turbulence effects, Ph.D. Dissertation, Cornell University, 265 pp.